Multiple-quantum excitation probabilities of Einstein-like modes of surface adsorbates induced by He-atom scattering

2002 J. Phys.: Condens. Matter 14 6233

(http://iopscience.iop.org/0953-8984/14/24/317)

INSTITUTE OF PHYSICS PUBLISHING JOURNAL OF PHYSICS: CONDENSED MATTER

J. Phys.: Condens. Matter **14** (2002) 6233–6261 PII: S0953-8984(02)36146-0

Multiple-quantum excitation probabilities of Einstein-like modes of surface adsorbates induced by He-atom scattering

J R Manson[1], **Andrew P Graham**[2,3] **and Mubing Li**[1]

[1] Department of Physics and Astronomy, Clemson University, Clemson, SC 29634, USA
[2] Max Planck Institut für Strömungsforschung, Bunsenstraße 10, D-37073 Göttingen, Germany

Received 23 April 2002
Published 31 May 2002
Online at stacks.iop.org/JPhysCM/14/6233

Abstract

Experimental data exhibiting multiple-quantum excitation of the vibrational modes of decoupled, oscillating adsorbates on a surface via impact by a He atom are reviewed for the cases of carbon monoxide and heavy rare gases adsorbed on metal substrates. The experimental scattering spectra are analysed using a dynamical scattering model that predicts correctly the angular dependences of the distributions of multiphonon excitations and the variation with incident energy and adsorbate frequency. The agreement between experiment and theory indicates that the details of the He–surface interaction potential are relatively unimportant for incident energies much higher than the vibrational energy. The model is used to predict the excitation probabilities of other possible vibrational modes which have not yet been observed using helium-atom scattering.

1. Introduction

Atomic and molecular adsorbates on surfaces often give rise to localized Einstein-like dispersionless phonon modes. In the case of isolated, non-interacting adsorbates such modes arise from the frustrated translation both normal and parallel to the surface, as well as from internal molecular modes. The principal examples of such systems are CO adsorbates on metal surfaces, particularly under conditions of very dilute coverage [1]. However, even in the case of a complete adsorbate monolayer, the frustrated translational motion normal to the surface (S-mode) often remains a dispersionless mode to a very large degree, since the relative displacement of the adsorbates parallel to the surface is of second order in the vertical displacement. Examples of such systems are readily found in the case of monolayers of rare gases on close-packed metal surfaces [1–5].

Processes of multiple-surface-phonon excitation are an important step in the accommodation of impact energy in atom–surface and molecule–surface interactions [6].

[3] Present address: Infineon Technologies AG, Corporate Research, Otto-Hahn-Ring 6, D-81730 Munich, Germany.

These processes aid in the sticking of particles on the surface and are crucial to heat transfer between the gas and solid phases, particularly at high temperature and for large particle mass [7]. Many studies have been performed for scattering from clean, well-ordered surfaces, particularly using helium-atom scattering (HAS), where the surface phonon modes are dispersive, resulting in broad energy transfer distributions [8]. On the other hand, a substantial number of HAS studies have shown that, with only a small fraction of the surface covered with adsorbed molecules or atoms, the phonon characteristics of the surface become dominated by dispersionless, Einstein-like phonon modes due to vibrations of the isolated or decoupled adsorbates [4, 9–11]. This arises because these modes often have frequencies lower than the zone-boundary frequency of the clean-surface Rayleigh and in-plane phonon branches, and so are easier to excite and annihilate during the scattering process for a large range of momentum transfers. In addition, the low frequency of these modes facilitates multiple excitation (multiphonon transfer) which manifests itself as overtones of the fundamental frequency in energy-resolved experiments.

Here, we review investigations of the angular distributions of multiphonon energy transfer processes involving adsorbed molecules for a range of incident conditions. A simple theoretical model is used to analyse the experimental HAS results for carbon monoxide adsorbed on both the Cu(001) and Pt(111) surfaces [12], and for a monolayer of Kr adsorbed on Pt(111). For these systems all of the vibrational and adsorption parameters have been well characterized. The scattering model considers the momentum transferred to adsorbed molecules or atoms with a hard-core potential by assuming that the helium atom imparts a short-duration impulse. In this way, very few assumptions need to be made about the shape of the adsorbates, or the interaction potential of the surface and the helium atom. In fact, for the case of CO adsorbates the potential contains no freely adjustable parameters, and for the Kr monolayers only a small number of parameters are needed. Thus, the lack of significant deviations of the measured scattered intensities from the predictions of this model indicate that the details of the interaction potential are relatively important.

The adsorption of CO on Cu(001) [11,13–16] and Pt(111) [10,17–19] has been extensively studied and the vibrational frequencies and details of the scattering from isolated molecules have been measured. In both cases, at low coverage, the CO molecule adsorbs in a vertical configuration with the carbon atom closest to the surface on top of a surface atom. Of particular interest in the present case is the parallel frustrated translation mode, or T-mode, which has a frequency of $\hbar\omega = 4$ meV for CO/Cu(001) and $\hbar\omega = 6$ meV for CO/Pt(111), about a factor of 8–9 lower than the frequency of the next mode which in both cases is the frustrated rotation. For comparison the frequencies and assignments of the various modes and other useful quantities are given in table 1. In the present study the multiple excitations of the T-mode are investigated for a range of incident angle and energy combinations. The angular data provide useful information on the scattering form factor, or shape of the CO molecule, with respect to the hard-core incoherent scatterer used in the calculation, whereas the energy dependence focuses on the range of available overtones which is related to the Bose and Debye–Waller factors. The differing frequencies of the CO T-mode vibration on Cu(001) and Pt(111) also test the applicability of this approach.

In the case of the rare-gas monolayer, the Kr frustrated translational mode perpendicular to the Pt(111) surface has an energy of 3.8 meV, well below the Brillouin zone-boundary energies of any of the Pt(111) substrate modes. Thus, for a large range of parallel momentum transfers, the scattered He-atom spectrum is completely dominated by multiphonon excitation of the S-mode.

The simplicity of the present theoretical explanation allows a straightforward interpretation of the dependence of the mode spectrum on the momentum transfer, both parallel and

Table 1. Comparison of the vibrational frequencies and other physical properties of carbon monoxide adsorbed on the Cu(001) and Pt(111) surfaces.

Property	Designation	CO/Cu(001)	CO/Pt(111)
Frequencies		$\hbar\omega$	$\hbar\omega$
C–O stretch	ν_1	258 meV [13]	261 meV [17]
M–CO stretch	ν_2 (S)	42.8 meV [13]	58 meV [17]
CO rotation	ν_3 (R)	35.3 meV [13]	51 meV [18]
CO translation	ν_4 (T)	3.94 meV [11]	6 meV [10]
Adsorption site		On top	On top
Adsorption energy	E_{ads}	0.7 eV [14]	1.5 eV [18]
Onset of desorption	T_{des}	150 K	400 K [18]
Diffusion barrier	E_{diff}	32 meV [15]	130 meV [19]

perpendicular to the surface. This momentum dependence is clearly related to the polarization of the mode, and shows that He-atom scattering can readily distinguish adsorbate surface mode polarizations. This approach also leads to a better understanding of the energy transfer between a gas and a weakly bound adsorbate layer on a substrate surface. The semiclassical theory used here shows that the present systems are still very quantum mechanical in nature, in spite of the fact that many quanta of energy are exchanged, since individual quantum excitations are clearly observed. In this sense, these experiments are intermediate between purely single-quantum situations and the classical multiphonon regime which is more typical for room temperature processes, for instance scattering from organic films [20] or heavy rare gases scattering from metal surfaces [21].

Below, the details of the helium scattering apparatus are presented in section 2 followed by the experimental results in section 3. The scattering theory is detailed in section 4 and then compared with the experimental results in section 5. Section 6 is a discussion of theoretical predictions for conditions under which the higher-energy vibrational modes might be observed, and the main conclusions are summarized in section 7.

2. Experimental details

The HUGO II high-resolution HAS apparatus, which is described in detail elsewhere [22, 23], incorporates a supersonic helium-atom beam source, with a velocity spread of $\Delta v/v \lesssim 1\%$, a target chamber which has a base pressure of better than 5×10^{-11} mbar, and a time-of-flight (TOF) arm of 1.4 m length at a fixed total scattering angle of $\theta_{SD} = 95.8^\circ$ with respect to the incident beam. The incident beam energy can be varied between 4 meV and 100 meV by changing the nozzle temperature between 19 and 450 K, and the nozzle pressure P_0 is optimized between about 5 and 250 bar to obtain the best velocity resolution.

For structural studies the elastic diffraction patterns can be measured for the two orthogonal components of the parallel momentum transfer in the surface plane, ΔK_x and ΔK_y. This is achieved by rotating the sample in the scattering plane by an angle $\Delta\theta$ away from the specular (polar angle) and by tilting it by an angle ϕ out of the scattering plane (tilt angle):

$$\begin{aligned} \Delta K_x &= -2k_i \sin(\Delta\theta)\cos(\theta_{SD}/2) \\ \Delta K_y &= k_i \sin(\phi)[\cos(\theta_{SD}/2 - \Delta\theta) + \cos(\theta_{SD}/2 + \Delta\theta)], \end{aligned} \tag{1}$$

where k_i is the incident momentum of the helium atoms. Thus, the complete 2D parallel reciprocal-lattice momentum transfer space can be mapped out in a simple way by systematically changing $\Delta\theta$ and ϕ with the sample manipulator.

The phonon dispersion curves were obtained from TOF measurements in which the helium-atom beam is chopped into short-duration pulses (10–20 μs) using a mechanical chopper placed in the beamline between the nozzle and the crystal. The momentum transfers corresponding to the inelastic peaks, measured for a given incident angle in the TOF spectra, were determined using the 'scan curve' relationship in the scattering plane:

$$\Delta K = k_f \sin(\theta_{SD} - \theta_i) - k_i \sin\theta_i, \tag{2}$$

where $\theta_i = \theta_{SD}/2 + \Delta\theta$ for in-plane scattering ($\phi = 0$). Typical measuring times for a TOF spectrum were about 60 min.

The Cu(001) and Pt(111) crystals were oriented to better than 0.25°, mechanically polished, and then cleaned *in situ* with cycles of sputtering with Ar^+ ions and annealing until a sharp He specular peak and low diffuse elastic intensities were observed. No impurities could be detected using Auger spectroscopy to within the detection limit of $\Theta \sim 0.01$, measured with respect to the density of clean-surface atoms. The sample temperature was controlled to much better than ± 1 K with an estimated absolute accuracy of ± 5 K using a Ni–CrNi (K-type) thermocouple attached to the side of the crystal. Sample cooling to <25 K was provided via a liquid-helium cold finger.

For most of the present CO measurements the dosage was below 0.23 l corresponding to a CO coverage of $\Theta_{CO} = 0.028$, as determined by the attenuation of the specularly reflected intensity [24]. Typical measuring times for a TOF spectrum were of the order of 5–30 min.

The preparation of the krypton monolayers has been described in detail elsewhere [5]. Krypton[4] was backfilled into the target chamber at a pressure of about 10^{-8} mbar with the crystal at a temperature of $T_S = 63$ K until one monolayer had been adsorbed and then the backfilling was stopped. This temperature is above the desorption temperature for more than one monolayer. The crystal was maintained at this temperature for 10 min to allow the remaining background krypton to pump away before the crystal was cooled to the measurement temperature. The krypton monolayer structure obtained using this method is described elsewhere [5].

3. Results

First, we discuss the observation of frustrated translational modes arising from dilute coverages of adsorbed CO. Most measurements were done on the Cu(001) surface and some experiments were carried out on a Pt(111) surface. In order to investigate the intensity distribution and incident energy dependence of the multiphonon processes, a large number of TOF spectra were measured for a range of incident conditions. In particular the CO/Cu(001) surface was studied because this system is well understood and the T-mode frequency has been measured in a number of studies [11, 15, 16, 25, 26]. To begin with, it is important to determine whether the CO coverage has an influence on the multiphonon intensities because effects of clustering were observed at low coverages in a recent study [15]. In figure 1 a series of TOF spectra, converted to energy transfer, are shown for several different coverages of CO ranging from $\Theta_{CO} = 0.005$ to $\Theta_{CO} = 0.088$. As the coverage increases another peak can be seen, in addition to the T-mode multiphonons at $\Delta E \approx \pm n \times 4$ meV, at $\Delta E \approx 5.2$ meV. A previous study [15] indicated that this peak is due to interactions between CO molecules in close proximity, i.e., due to small CO clusters on the surface. This peak becomes significant at coverages above $\Theta_{CO} \approx 0.05$ ((d), (e)).

To investigate whether the clustering influences the intensity ratio of the fundamental and overtones of the T-mode the intensities of the fundamental energy loss ($\Delta E = -4$ meV) and

[4] Gases supplied by Messer Griesheim, Krefeld, Germany, with a purity of 99.99%.

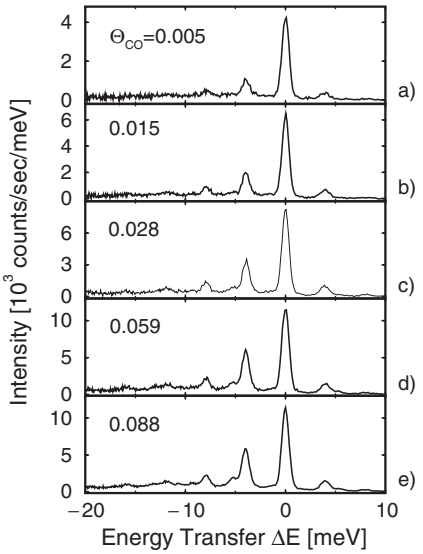

Figure 1. A series of HAS inelastic TOF spectra, converted to an energy transfer scale, for a range of CO coverages on Cu(001) at $T_S = 50$ K. The incident energy was 40.3 meV directed along the Cu(001) [100] azimuth at an incident angle of $\theta_i = 28.2^\circ$ in a fixed geometry in which $\theta_f = \theta_{SD} - \theta_i$ with $\theta_{SD} = 95.8^\circ$. The peaks at multiples of $\Delta E = \pm 4$ meV are attributed to the excitation of the T-mode of isolated CO molecules adsorbed at on-top sites and become stronger with increasing coverage. An additional peak at $\Delta E = -5.2$ meV is visible at higher coverages above $\Theta_{CO} \approx 0.05$ ((d), (e)) which is assigned to excitations of small CO clusters.

the first-overtone ($\Delta E = -8$ meV) peaks were extracted from the spectra in figure 1. The intensities are shown in figure 2. The intensities of the fundamental and first overtone exhibit a nearly linear increase with coverage up to $\Theta_{CO} \approx 0.03$ above which the rate of increase is lower, with saturation beginning above $\Theta_{CO} > 0.06$. Across the whole coverage range studied, the intensity ratio of the fundamental and first overtone remains approximately constant at 3. The linear increase is consistent with a simple increase in the density of scattering centres on the surface. The deviation from the linear behaviour at coverages $\Theta_{CO} > 0.03$ can be interpreted as scattering involving more than one scattering centre (CO molecule) due to close proximity. Thus, in order to avoid any coverage effects a coverage of less than $\Theta_{CO} \approx 0.03$ is necessary. We used a CO coverage of $\Theta_{CO} = 0.028$ for all of the following measurements.

Figure 3 shows several typical TOF spectra measured with an incident beam energy of 66.6 meV and a surface temperature of $T_S = 50$ K for a range of incident angles for $\Theta_{CO} = 0.028$ on Cu(001). The spectra show that the total scattered intensity decreases quickly for incident angles far from the specular peak ($\theta_i = 47.9^\circ$), as also shown in several previous studies [25,27,28]. At the same time, multiples of the fundamental T-mode frequency for CO/Cu(001) of $\hbar\omega \approx 4$ meV [11, 15] are observed to become much more dominant with the third overtone clearly visible at $\Delta E \approx -16$ meV.

The number of overtones excited becomes significantly larger for higher incident energies, as shown in figure 4. In this case the incident angles are approximately the same but the beam energy increases from 20.0 to 83.5 meV for the same surface temperature of $T_S = 50$ K and CO coverage $\Theta_{CO} = 0.028$. At 20.0 meV three energy loss peaks can be detected whereas at 83.5 meV the seventh energy loss peak (sixth overtone) is clearly visible and the eighth peak is just visible above the noise. Thus, the number of excitations is not directly proportional

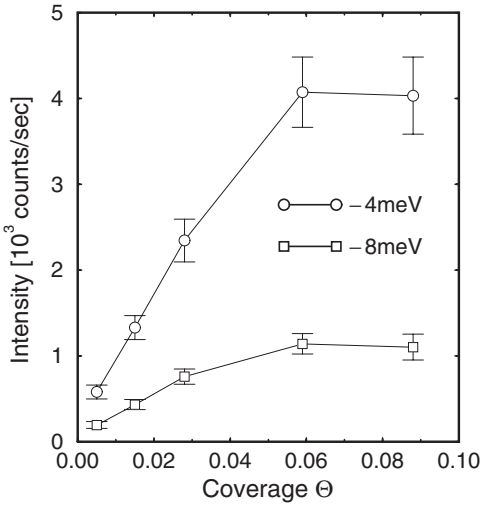

Figure 2. T-mode fundamental ($n = -1$) and first-overtone ($n = -2$) energy loss intensities as a function of surface coverage for an incident energy of 40.3 meV and an angle of $\theta_i = 28.2^\circ$. The intensities show similar monotonic increases with a constant ratio of $I_{n=-1}/I_{n=-2} \approx 3$ up to a coverage of $\Theta_{CO} \approx 0.06$ followed by a slight intensity decrease.

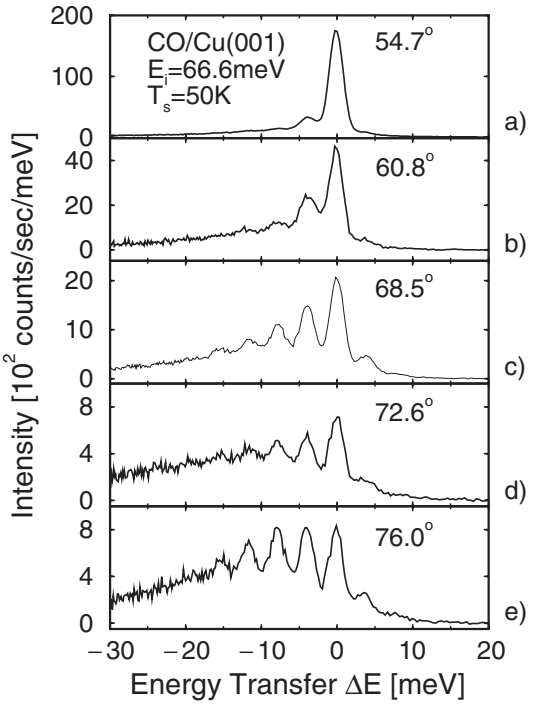

Figure 3. Several helium TOF spectra, converted to an energy transfer scale, for a CO coverage of $\Theta_{CO} = 0.028$ on Cu(001) and a range of incident angles θ_i with $\theta_f = \theta_{SD} - \theta_i$. The surface temperature was $T_S = 50$ K and the incident energy was $E_i = 66.6$ meV. Multiple excitations of the T-mode peak at $\Delta E = \pm n \times 4$ meV become dominant features of the spectra as the incident angle is increased.

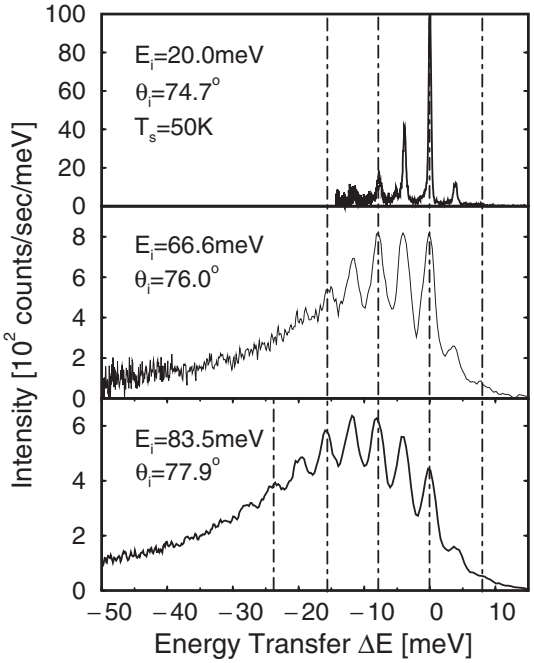

Figure 4. Spectra as in figure 3 at several incident energies of $E_i = 20.0$, 66.6, and 83.5 meV. The surface temperature was $T_S = 50$ K and the incident angle is approximately constant in the range $\theta_i = 74.7°$–$77.9°$. At 20 meV the second overtone of the $\Delta E = -4$ meV T-mode peak at $\Delta E = -12$ meV is just visible whereas the seventh overtone is observed for an incident energy of 83.5 meV.

to the incident beam energy. However, higher overtones may be hidden by the increased background level and resulting statistical noise which is due to the enhanced Cu(001) surface multiphonon processes at the higher beam energies [23]. It is also worthwhile noting that the measured multiphonon excitations are perfectly harmonic up to the seventh overtone, to within experimental error. This provides some clues as to the nature of the interaction of the helium atoms with a surface, as will be discussed later.

In addition to the measurements of CO/Cu(001), TOF spectra were obtained for a low coverage ($\Theta_{CO} \approx 0.03$) of CO on Pt(111) under similar scattering conditions. The CO/Pt(111) T-mode frequency was determined in earlier measurements [10, 19] to be $\hbar\omega = 6$ meV, 50% higher than for CO/Cu(001) and, thus, provides a useful comparison. Figure 5 compares TOF spectra measured under nearly identical scattering and temperature conditions for $\Theta_{CO} \approx 0.03$ CO on Cu(001) and Pt(111). The spectra for CO/Pt(111) exhibit fewer overtones than for CO/Cu(001), as expected for the higher vibrational frequency. However, the distributions of intensity with energy transfer (intensity envelope) are similar in the two cases, taking into account the larger peak width of the CO/Pt(111) T-mode vibration due to the shorter lifetime [19] compared to CO/Cu(001) [15]. Also shown in figure 5 as solid curves are the theoretical calculations as discussed below in section 5.

The case of the S-modes of a monolayer of Kr adsorbed on a Pt(111) substrate presents many similarities to that of the CO adsorbates discussed above, but there are also some significant differences. Figure 6 shows a series of TOF measurements for one monolayer of krypton on Pt(111) at an incident beam energy of $E_i = 25.1$ meV and a surface temperature of $T_S = 58$ K and several incident angles. As in the case of the frustrated translational modes

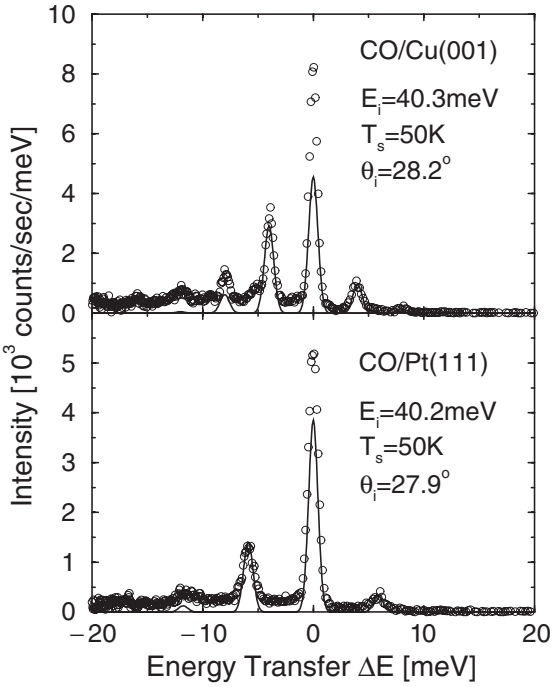

Figure 5. Comparison between the TOF spectra for helium scattered from CO on Cu(001) and Pt(111). The scattering conditions are nearly identical; the incident energies are 40.3 and 40.2 meV, and the incident angles are $\theta_i = 28.2^\circ$ and 27.9° for CO/Cu(001) and CO/Pt(111), respectively. The coverage was $\Theta_{CO} \approx 0.03$ and the surface temperature $T_S = 50$ K in both cases, and the spectra have been converted from flight time to energy transfer. Note that the peak width for the CO/Pt(111) T-mode at $\Delta E = -6$ meV is larger than for CO/Cu(001) due to the shorter vibrational lifetime. The solid curves are the calculations discussed in section 5.

of adsorbed CO, in addition to the elastic peaks at $\Delta E = 0$, a number of inelastic peaks are observed for both energy loss and gain. The energy transfer of these inelastic peaks does not vary with incident angle and corresponds to multiples of the known Kr/Pt(111) monolayer perpendicular vibrational mode (S-mode) at $\Delta E = \pm n \times 3.8$ meV [29].

The intensities of the inelastic peaks change significantly with the incident angle. The peaks are most intense close to the specular peak position at $\theta_i = 47.9^\circ$ and fall off rapidly as the incident angle is increased or decreased away from the specular. The total number of observed peaks, however, is the same at all measured angles, in contrast to the case for CO.

TOF measurements were also made at a higher incident energy of 43 meV for the same surface temperature, as shown in figure 7. The dispersionless Kr monolayer S-mode peaks at $\Delta E = \pm n \times 3.8$ meV are clearly visible in all spectra up to the $n = 5$ phonon creation peak at $\theta_i = 32.9^\circ$. Due to the higher incident energy the smooth inelastic background due to multiphonon excitation of the dispersive modes is more dominant than for $E_i = 25.1$ meV.

4. Theory

4.1. Differential reflection coefficient

A starting point for a treatment of inelastic scattering between a projectile and a many-body target is the quantum mechanical transition rate, or generalized Fermi golden rule, for the

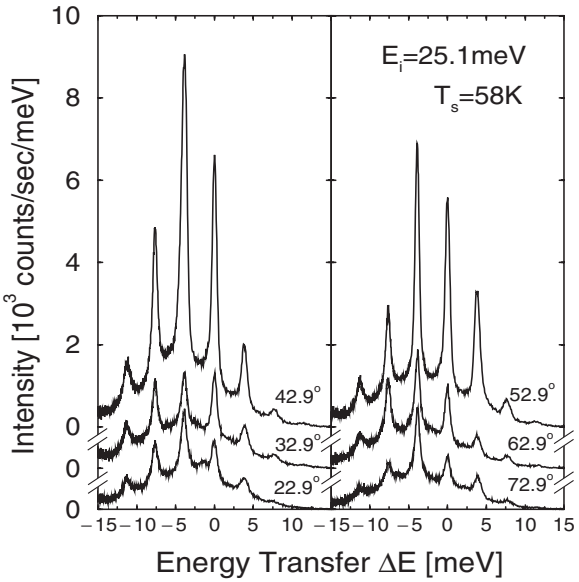

Figure 6. Several energy-resolved spectra for one monolayer of krypton on Pt(111) at a surface temperature of $T_S = 58$ K and an incident beam energy of $E_i = 25.1$ meV. The beam was aligned along the Pt [11$\bar{2}$] azimuth and the incident angle θ_i is shown beside each curve. The peaks at multiples of $\Delta E = \pm n \times 3.8$ meV (n is an integer) correspond to excitations of the dispersionless perpendicular (S-mode) vibrations of the Kr monolayer which are observed for both energy loss and gain.

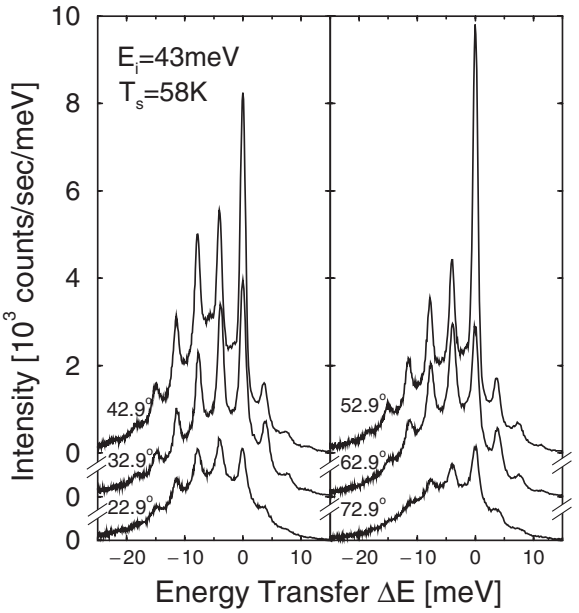

Figure 7. As figure 6, except for an incident beam energy of $E_i = 43.0$ meV.

projectile scattering from the initial state of wavevector $\boldsymbol{k}_i$ to the final state $\boldsymbol{k}_f$ which is given by [31, 32]

$$w(\boldsymbol{k}_f, \boldsymbol{k}_i) = \left\langle \frac{2\pi}{\hbar} \sum_{\{n_f\}} |\langle n_f, \boldsymbol{k}_f | \mathcal{T} | \boldsymbol{k}_i, n_i \rangle|^2 \delta(\mathcal{E}_f - \mathcal{E}_i) \right\rangle \tag{3}$$

where $|n_i\rangle$ is the initial many-body state of the unperturbed target, $\sum_{\{n_f\}}$ is a summation over all final states of the target, $\mathcal{T}$ is the transition operator, $\mathcal{E}_f$ and $\mathcal{E}_i$ are respectively the final and initial energy of the entire system of target plus projectile, and the braces $\langle\ \rangle$ signify an average over all initial target states. In atom–surface scattering the measured intensities are usually differential reflection coefficients which are obtained from the transition rate $w(\boldsymbol{k}_f, \boldsymbol{k}_i)$ on multiplication by the density of final scattering states as follows:

$$\frac{\mathrm{d}R}{\mathrm{d}\Omega_f\, \mathrm{d}E_f} = \frac{L^4}{(2\pi\hbar)^4} \frac{m^2 |\boldsymbol{k}_f|}{k_{iz}} w(\boldsymbol{k}_f, \boldsymbol{k}_i) \tag{4}$$

where m is the mass of the projectile atom and k_{iz} is the component of the incident wavevector perpendicular to the surface.

A general expression for the transition rate for the full transition operator can be obtained in the semiclassical limit. This involves making the approximation that the collision is fast in comparison to phonon periods and that it is sufficient to expand the interaction potential through terms linear in the atomic displacements. These approximations have been justified in detail in connection with development of multiphonon exchange in atom–surface scattering, and have been shown to be valid through extensive comparison with experimental measurements [32–35]. The result is the following form for the transition rate:

$$w(\boldsymbol{k}_f, \boldsymbol{k}_i) = \frac{1}{\hbar^2} |\tau_{fi}|^2 \mathrm{e}^{-2W(\boldsymbol{k}_f, \boldsymbol{k}_i)} \int_{-\infty}^{+\infty} \mathrm{d}t\, \mathrm{e}^{-\mathrm{i}(E_f - E_i)t/\hbar} \mathrm{e}^{Q(\boldsymbol{k}_f, \boldsymbol{k}_i; t)} \tag{5}$$

where $Q(\boldsymbol{k}_f, \boldsymbol{k}_i; t)$ is a generalized displacement correlation function, and $2W(\boldsymbol{k}_f, \boldsymbol{k}_i) = Q(\boldsymbol{k}_f, \boldsymbol{k}_i; t = 0)$ [35]. In the semiclassical approximation of quick collisions, i.e., collision times which are short compared to a vibration period, the time-dependent correlation function $Q(\boldsymbol{k}, t)$ becomes the displacement correlation function

$$Q(\boldsymbol{k}_f, \boldsymbol{k}_i; t) \longrightarrow Q(\boldsymbol{k}, t) = \langle \boldsymbol{k} \cdot \boldsymbol{u}(\boldsymbol{0})\, \boldsymbol{k} \cdot \boldsymbol{u}(\boldsymbol{t}) \rangle, \tag{6}$$

where $\boldsymbol{k} = \boldsymbol{k}_f - \boldsymbol{k}_i$ is the scattering vector and the argument of the Debye–Waller factor is

$$2W(\boldsymbol{k}) = Q(\boldsymbol{k}, t = 0) = \langle (\boldsymbol{k} \cdot \boldsymbol{u}(\boldsymbol{0}))^2 \rangle. \tag{7}$$

In equation (5) the energies E_f and E_i are, respectively, the final and initial kinetic energies of the scattered projectile. The factor $|\tau_{fi}|^2$ is the form factor which depends on the nature of the scattering centre and the interaction potential. The form factor is discussed in more detail in section 4.2.

In the case of a vibrational displacement having only a single dispersionless Einstein mode of frequency ω, equations (5) and (6) can be evaluated together and the result is a generalized temperature-dependent Poisson series which produces the multiphonon overtones [36]. This expression appears as follows:

$$\begin{aligned} \frac{\mathrm{d}^3 R(\boldsymbol{k}_f, \boldsymbol{k}_i)}{\mathrm{d}E_f\, \mathrm{d}\Omega_f} = {} & \frac{m^2}{(2\pi\hbar)^4} \frac{|\boldsymbol{k}_f|}{k_{iz}} |\tau_{fi}|^2 \mathrm{e}^{-2W(\boldsymbol{k})} \mathrm{e}^{-2W_T(\Delta K)} \\ & \times \sum_{\alpha=-\infty}^{+\infty} I_{|\alpha|}\left(\frac{\Delta K^2 \hbar}{M_A \omega} \sqrt{n(\omega)[n(\omega)-1]} \right) \left(\frac{n(\omega)}{n(\omega)-1} \right)^{\alpha/2} \delta(E_f - E_i - \alpha\hbar\omega) \end{aligned} \tag{8}$$

where $I_\alpha(z)$ is the modified Bessel function of order α, $|\tau_{fi}|^2$ is the form factor, ΔK is the component of $\boldsymbol{k}$ in the direction of the mode polarization, M_A is the effective mass derived from the normal-mode analysis of the CO adsorbate as shown in section 4.3, and $n(\omega)$ is the Bose–Einstein function given by

$$n(\omega) = \frac{1}{\mathrm{e}^{\hbar\omega/k_B T_S} - 1}. \tag{9}$$

The Debye–Waller factor arising from the contribution of the adsorbate Einstein mode is given by

$$2W_S(\Delta K) = \frac{\hbar\,\Delta K^2}{2M_A\omega}\left[n(\omega) + \frac{1}{2}\right]. \tag{10}$$

The Debye–Waller factor arising from the contributions of the substrate phonons is chosen to be that of a Debye phonon distribution:

$$2W(\boldsymbol{k}) = \frac{3\hbar\boldsymbol{k}^2}{M_C\omega_D^3}\int_0^{\omega_D} \mathrm{d}\omega\,\omega\left[n(\omega) + \frac{1}{2}\right], \tag{11}$$

where M_C is the mass of a substrate atom, and $\hbar\omega_D = k_B\Theta_D$ where Θ_D is the Debye temperature. In the limit of temperature T_S large compared to Θ_D, this reduces to the well-known expression

$$2W(\boldsymbol{k}) = \frac{3\hbar^2\boldsymbol{k}^2 T_S}{M_C k_B \Theta_D^2}. \tag{12}$$

The analysis of the scattering intensity measurements in this article is based primarily on equation (8) and we note that this result contains a full treatment of the adsorbate recoil within this semiclassical approximation and the zero-point motion is treated correctly throughout.

4.2. The form factor for adsorbed CO

In order to accurately calculate the peak intensities of isolated adsorbed CO, the choice of a suitable form factor, or adsorbate shape, needs to be considered. In the semiclassical limit, the form factor amplitude τ_{fi} is given by the transition matrix for scattering by the elastic part of the interaction potential extended off the energy shell [35], thus permitting the form factors derived from elastic scattering experiments and calculations to be used for the present inelastic scattering calculations. A complete form factor contains all of the details of the scattering interaction including multiple scattering from the adsorbate and surface, the He–adsorbate potential and the He–metal surface potential. These details typically make a full form factor difficult and time consuming to compute [37]. Fortunately, in previous work on the scattering of He atoms from adsorbed CO, it has been shown that both the elastic and inelastic scattering cross-sections are determined largely by scattering from the hard repulsive core of the CO. Furthermore, this core is well approximated by a hard hemisphere for the scattering of He from isolated CO on close-packed metal surfaces [27, 28, 38].

Using these established ideas, a simple model for the form factor for the present problem can be developed based on the scattering from a hard sphere. In standard treatments, the scattering from an isolated scattering centre is described by an asymptotic wavefunction of the form

$$\Psi_i \longrightarrow \mathrm{e}^{\mathrm{i}\boldsymbol{k}_i\cdot\boldsymbol{r}} + \frac{f(\theta,\phi)}{r}\mathrm{e}^{\mathrm{i}k_i r}. \tag{13}$$

For a hard sphere of radius a, the form factor $f(\theta)$, as a function of the scattering angle θ, is given by the following well-known expression in the Kirchhoff limit $k_i a \longrightarrow \infty$ [39]:

$$f(\theta) = -\frac{ia}{2}\left\{ i\exp\left(-2ik_i a \sin\frac{\theta}{2}\right) - k_i a\left(\frac{1+\cos\theta}{k_i a \sin\theta}\right) J_1(k_i a \sin\theta)\right\}, \qquad (14)$$

where $J_1(z)$ is the first-order Bessel function. The use of the Kirchhoff approximation is justified for the present case because the incident wavevectors range from roughly 6 to 12 Å^{-1} and the hard-core radius of the He–CO potential is about 2.3 Å; thus $k_i a > 10$ for all incident energies. The first term on the right-hand side of equation (14) is called the illuminated face contribution and it produces uniform scattering intensity at all angles, while the second term is the Fraunhofer contribution.

If the adsorbed CO is modelled by a hemisphere on an otherwise flat, mirror surface, then one must account for the possibility of double-scattering events involving scattering from the hemisphere plus a reflection with a concomitant phase change of π by the flat surface. This is readily effected by adding to equation (14) a second term which accounts for the processes of double scattering from the flat surface. For the simplest case of scattering in the sagittal plane, and for a fixed angle θ_{SD} between the incident beam and the detector direction, the scattering form factor becomes

$$f_S = f(\pi - \theta_{SD}) - f(\theta_f - \theta_i) \qquad (15)$$

where θ_i and θ_f are the incident and final scattering angles with respect to the surface normal, respectively.

The form factor corresponding to this model is given by $|\tau_{fi}|^2 \propto |f_S|^2$, which consists of an envelope governed by the Fraunhofer term at small parallel momentum transfer $\Delta\boldsymbol{K}$ and by the constant illuminated face contribution at large $\Delta\boldsymbol{K}$. It also contains interference terms called 'reflection symmetry oscillations' because of their similarity in origin to the symmetry oscillations observed in identical particle scattering [27].

An even simpler approximation to the form factor is to use only the envelope function, which is given by

$$|\tau_{fi}|^2 \propto \overline{|f_S(\theta)|^2} \propto \left\{1 + \frac{4\boldsymbol{k}_i^2}{\pi a}\frac{1}{|\Delta\boldsymbol{K}|^3}\right\}. \qquad (16)$$

This simple form factor combines the two essential features arising from hard-core scattering, which are the Fraunhofer contribution that varies as $|\Delta\boldsymbol{K}|^{-3}$, and the illuminated face contribution which is a constant. It is a function of both the final and initial energies through its dependence on the parallel momentum transfer $\Delta\boldsymbol{K}$. Equation (16) is the form factor which is used in the analysis of the CO data in section 5 below.

4.3. Normal-mode analysis for adsorbed CO

In order to obtain the effective mass M_A of the CO molecules for each of the vibrational modes a normal-mode analysis for the modes of CO adsorbed on a Cu(001) surface was made. A model adequate for the purposes of the analysis presented here is the simple ball-and-spring model shown in figure 8. This model leaves the vertical and horizontal motion of the carbon and oxygen atoms uncoupled. For vertical motion the spring of spring constant k_C^z represents the carbon–metal bond and a second with spring constant k_O^z represents the C–O bond. For the horizontal motion, springs with constants k_C^x and k_O^x connect the carbon and oxygen atoms, respectively, to the surface vertical, and a third k_a^x is an angle-bending spring which tends to restore the carbon and oxygen to a straight-line configuration with respect to the bonding point on the surface.

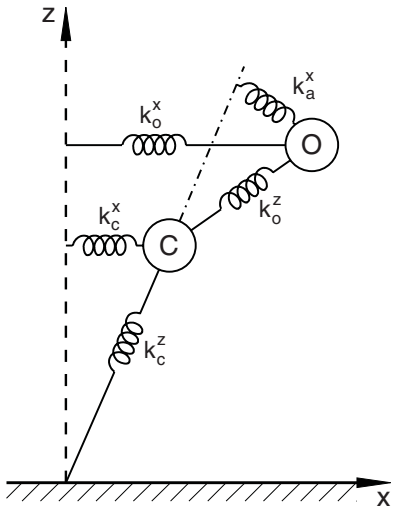

Figure 8. A schematic diagram of the 'ball-and-spring' model used for the normal-mode analysis for the vibrations of an isolated CO molecule. For the calculations presented here k_{O}^x was taken to be zero.

Table 2. Comparison of model calculations with experiment for the isotope shifts of the T- and R-mode frequencies for CO/Cu(001), with respect to the frequency of the $^{12}C^{16}O$ isotopomer, based on the model of figure 8.

	T-mode shift (%)		R-mode shift (%)	
Isotope	Expt [15]	Present calc.	Expt [15]	Present calc.
$^{12}C^{18}O$	−4.58	−2.64	−0.98	−1.68
$^{13}C^{16}O$	−0.76	−0.28	−3.12	−2.72
$^{13}C^{18}O$	−5.09	−3.76	−3.93	−4.46

The normal-mode analysis for such a system is straightforward. For the horizontally polarized modes, a satisfactory match of the 4 meV T-mode and the 35.3 meV R-mode is obtained with $k_{\mathrm{C}}^x = 620.7$ amu meV^2, $k_a^x = 6166.8$ amu meV^2 and $k_{\mathrm{O}}^x = 0$. These two frequencies can also be matched with a large range of values of $k_{\mathrm{O}}^x > 0$ with a concomitant small reduction in the values of the other two constants, but the simplest choice of $k_{\mathrm{O}}^x = 0$ has been used here. This model also predicts the measured isotope shifts in the frequencies well, as shown in table 2.

The relative sizes of the carbon and oxygen vibrational amplitudes are expressed in terms of the polarization vectors $e(\beta, \kappa, \nu)$, where β is the Cartesian direction index, κ is an integer denoting the atom, and ν is an integer denoting the mode number. For the low-frequency T-mode this model gives $e(x, \mathrm{O}, \mathrm{T})/e(x, \mathrm{C}, \mathrm{T}) = +1.67$, while for the R-mode it gives $e(x, \mathrm{O}, \mathrm{R})/e(x, \mathrm{C}, \mathrm{R}) = -0.719$.

The time-dependent displacement correlation function for a harmonic system such as this is given by

$$\langle u_\kappa^\beta(0) u_{\kappa'}^{\beta'}(t)\rangle = \sum_\nu \frac{\hbar}{2N\sqrt{M_\kappa M_{\kappa'}}\omega_\nu} e(\beta, \kappa, \nu) e^*(\beta', \kappa', \nu)\{[n(\omega_\nu)+1]\mathrm{e}^{-\mathrm{i}\omega\nu t} + n(\omega_\nu)\mathrm{e}^{+\mathrm{i}\omega\nu t}\}, \tag{17}$$

Table 3. Comparison of model calculations with experiment for the isotope shifts of the S-mode and C–O stretch-mode frequencies of CO/Cu(001), with respect to the frequency of the $^{12}C^{16}O$ isotopomer, based on our the model of figure 8.

	S-mode shift (%)		C–O stretch-mode shift (%)	
Isotope	Expt [15]	Present calc.	Expt	Present calc.
$^{12}C^{18}O$	−2.08	−3.58	—	−2.21
$^{13}C^{16}O$	−0.94	−1.61	—	−2.35
$^{13}C^{18}O$	−3.04	−5.02	—	−4.63

where M_κ is the mass of the κth atom, ω_ν is the frequency of the νth normal mode, and N is the total number of modes. Equation (17) shows that the effect of the polarization on expression (8) for calculating the intensities can be treated through introduction of an effective mass. As discussed above in section 4.2, the adsorbed CO molecule can be represented by a hard hemispherical profile, which derives mainly from the hard core of the oxygen atom, on a hard flat surface. This simplifies the calculation because it can be assumed that the only term of equation (17) which enters into the calculation of the Einstein mode intensities of equation (8) is the one for the time-dependent correlation of the oxygen atom with itself. The effective mass of the oxygen atom is $M_A = M_O/|e(x, O, \nu)|^2$, where M_O is the mass of an oxygen atom and, consequently, the effective mass for the T-mode can be taken to be $M_T = M_O/|e(x, O, T)|^2 = 16\ \text{amu}/0.859^2 = 21.7$ amu. Similarly, for the R-mode an effective mass of $M_R = M_O/|e(x, O, R)|^2 = 16\ \text{amu}/0.584^2 = 46.96$ amu can be obtained.

For the vertically polarized mode, a match to the 42.8 meV S-mode and the 258 meV C–O stretch mode is obtained with $k_C^z = 53,394$ amu meV^2 and $k_O^z = 437,781$ amu meV^2. Therefore the effective mass for the S-mode is $M_S = M_O/|e(z, O, S)|^2 = 16\ \text{amu}/0.721^2 = 30.02$ amu. The calculated isotope frequency shifts of the S-modes and C–O stretch modes are given in table 3.

4.4. The form factor for Kr monolayers

Following the use of a hard-core form factor for treating the inelastic scattering from isolated CO molecules, only the repulsive part of the He–surface interaction potential will be considered here. In the present case of a full monolayer coverage of a heavy rare gas the repulsive part of the interaction potential is, to a very good approximation, a decaying exponential function in the direction perpendicular to the surface, modified by a smooth corrugation parallel to the surface to account for the observed weak diffraction peaks [1]. Since the diffraction features observed in the present experiments were very weak [5], the corrugation of the surface repulsion will be ignored and the potential will be taken to be a simple exponential:

$$V(z) = V_0 e^{-\beta z}. \tag{18}$$

Such a purely repulsive potential as equation (18) neglects the attractive adsorption well caused by the van der Waals force in front of the surface. Since this attractive well is small for He interacting with metal or rare-gas surfaces, it can often be neglected if the incident energy is sufficiently large. Here, the attractive potential has been neglected also for a second reason, to avoid the introduction of an additional adjustable parameter, because it is desired to examine this system with the simplest form of theory that explains the basic physical processes.

For the exponential repulsive potential of equation (18) it has been shown that the transition matrix for inelastic scattering can be approximated by the product of a Jackson–Mott matrix element $v_{J-M}(k_{fz}, k_{iz})$, which is a function of the perpendicular momenta, and a

cut-off function which is a function of parallel momentum transfer $\Delta \boldsymbol{K}$ (the surface-parallel components of $\boldsymbol{k}$) as follows [40]:

$$\tau_{fi} = v_{J-M}(k_{fz}, k_{iz}) \exp\left\{ \frac{-\beta^2}{Q_0^2} \left(\left(1 + \left(\frac{\Delta \boldsymbol{K}}{\beta} \right)^2 \right)^{1/2} - 1 \right) \right\}. \tag{19}$$

The Jackson–Mott matrix element is the matrix element of the exponential potential of equation (18) taken with respect to its own one-dimensional distorted wave eigenfunctions. Defining the dimensionless perpendicular momenta as $q = k_{iz}/\beta$ and $p = k_{fz}/\beta$ it is given by [41, 42]

$$v_{J-M}(p, q) = \frac{p - q}{\sinh(p - q)} \frac{p + q}{\sinh(p + q)} \left\{ \frac{\sinh(2p) \sinh(2q)}{4pq} \right\}^{1/2}. \tag{20}$$

The two parameters, β of the Jackson–Mott matrix element, and Q_0 of the cut-off factor, will be used as the only adjustable parameters to fit the data.

A normal-mode analysis for the Kr S-modes is not needed because each Kr atom vibrates independently of the others and coupling to the substrate modes is small. The effective mass is then the same as the Kr atomic mass.

The only other parameter not yet completely specified is the substrate Debye temperature that appears in $W(\boldsymbol{k})$ of equation (11), but as stated previously this cannot be considered an adjustable parameter because its value in the case of He-atom scattering from Pt(111) has been determined from independent measurements to be approximately $\Theta_D = 230$ K [43] and this value will be used in the analysis presented below.

5. Analysis of the data

5.1. Intensities of He-atom scattering from CO adsorbates

Since in the present work we are mainly interested in the probabilities for inelastic scattering from the adsorbed molecules, the broad substrate multiphonon background under the adsorbate vibrational peaks was subtracted from the experimental TOF spectra to leave just those peaks. This was accomplished by subtracting a smooth curve fitted to the intensity between the adsorbate inelastic peaks from each spectrum. The resulting background-subtracted data is shown in figures 9–12.

In order to test the hypothesis that the form factor for inelastic scattering from CO on metal surfaces can be approximated by simple scattering from a hard hemisphere the calculations using equation (8) were first performed for a constant form factor $|\tau_{fi}|^2 = 1$. To compare the results of the calculations, which are a series of energy δ-function peaks, with the experimental measurements, the calculated spectra were broadened with a fixed-width Gaussian function, where the width was fitted to the experimental resolution. These calculations were fitted to the background-subtracted data by multiplying each calculation by a normalization coefficient, where the intensity matching was made, in most cases using the fundamental energy loss peak (i.e., the $n = -1$ phonon creation peak). This results in a fit to the experimental data which, for each individual TOF spectrum, is essentially a zero-parameter fit. This is because the differential reflection coefficient of equation (8) with a constant form factor has no adjustable parameters aside from the Debye–Waller temperature appearing in the substrate Debye–Waller factor $2W_S(\boldsymbol{k})$.

The resulting normalization coefficients, which contain information about the form factor, are shown for each of the four incident energies in figure 13. Presented alongside the coefficient points in figure 13 are the form factor curves derived using equation (16) and a

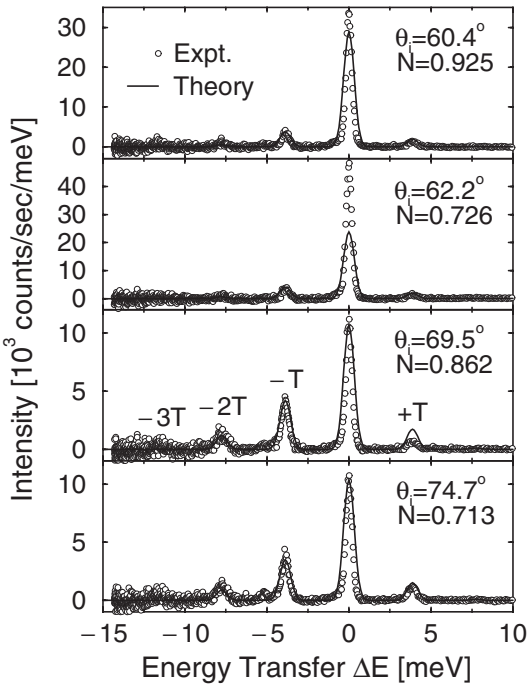

Figure 9. A series of HAS inelastic TOF spectra, converted to an energy transfer scale, for $\Theta_{CO} = 0.028$ CO on Cu(001) at $T_S = 50$ K. The incident energy was 20.0 meV. The incident angles range from $\theta_i = 60.4^\circ$ to 74.7° with $\theta_f = 95.8^\circ - \theta_i$ directed along the Cu(001) [100] azimuth. The experimental points are shown as circles while the solid curves are the results of the theory.

radius of $a = 2.3$ Å (solid curves). This value of the radius is well established from previous investigations of the elastic scattering of He from CO on Cu(001) and other metal substrates [28] and, consequently, a cannot be considered to be a freely variable parameter. The simple form factor given by equation (16) matches the trend of the normalization points quite well for all four incident energies. It is seen that for scattering at incident angles near to the specular condition at $\theta_i = 47.9^\circ$ the intensity rises sharply due to the $|\Delta \boldsymbol{K}|^{-3}$ term at small $\Delta \boldsymbol{K}$ in the form factor, while for large incident angles the intensity saturates to a smaller constant value which can be attributed to the illuminated face contribution from the hard-core scattering. Thus, the observed angular intensity dependences are well represented by the form factor in equation (16) justifying its use together with equation (8) to simulate the TOF spectra including the momentum transfer dependences of the intensities.

The results of the complete calculations are shown in figures 9–12 (solid curves). In the process of this final calculation with the new form factor it was still found to be necessary to multiply each calculated curve by a renormalization factor N close to unity in order to obtain the best fit. The need for this final renormalization is obvious from figure 13 because, although the calculated form factor of equation (16) follows the observed intensities quite well, the points are scattered about the theoretical curve. The value of the final renormalization constant is shown in each TOF plot. It is seen that these final calculations with the form factor of equation (16) agree rather well with all of the TOF experimental data measured.

The reason for the residual fluctuations of the inelastic intensities compared with those calculated using the simple form factor is well understood: the characteristic signature of scattering from an isolated adsorbate, whether elastic or inelastic, is a supernumerary rainbow

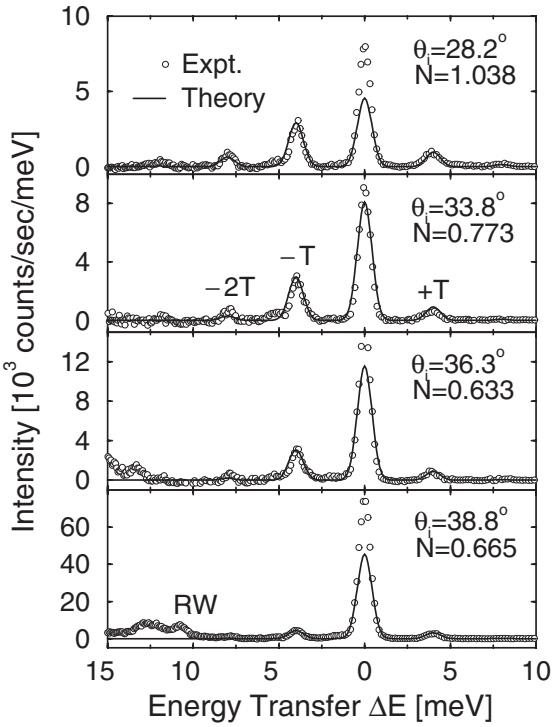

Figure 10. As figure 9, except with the incident energy at 40.29 meV, and incident angles from $\theta_i = 28.2^\circ$ to 38.8°.

oscillation in the differential reflection coefficient caused by multiple scattering between the adsorbate and the surface substrate [25, 27, 28, 38]. These oscillations are 'reflection symmetry oscillations' and they are most easily observed in experiments which follow the intensity of a single selected multi-quantum overtone peak as a function of parallel momentum transfer $\Delta \boldsymbol{K}$. They also affect the measured results in this current set of experimental measurements. However, because the current observations were taken at rather widely separated values of incident angles, the measurements are not sufficiently dense to exhibit these oscillations. The small differences appearing in figure 13 are clearly due to these oscillations about the envelope function given by equation (16) which explicitly excludes these reflection symmetry oscillations.

In figures 9–12 it is apparent that often the experimentally measured zero-loss peak is substantially larger than the calculation. This is because contributions to this peak come also from other sources, for example the diffuse elastic scattering from defects and other impurities on the surface.

The importance of the form factor is illustrated in figure 14 which shows TOF spectra for $E_i = 40.29$ meV at three different incident angles. The left-hand panels show the background-corrected data together with calculations using a constant form factor $\tau_{fi} = 1$, while the right-hand panels show the same data with calculations obtained with the form factor given by equation (16). The two peaks in the experimental data marked L and R are, respectively, the longitudinal resonance and the Rayleigh mode arising from the substrate vibrations. At the incident angle of $\theta_i = 28.2^\circ$ which is far from the specular position and where the parallel momentum transfers for all observable overtone peaks are rather large (and hence the form factor of equation (16) is nearly constant), there is little difference between the two calculations.

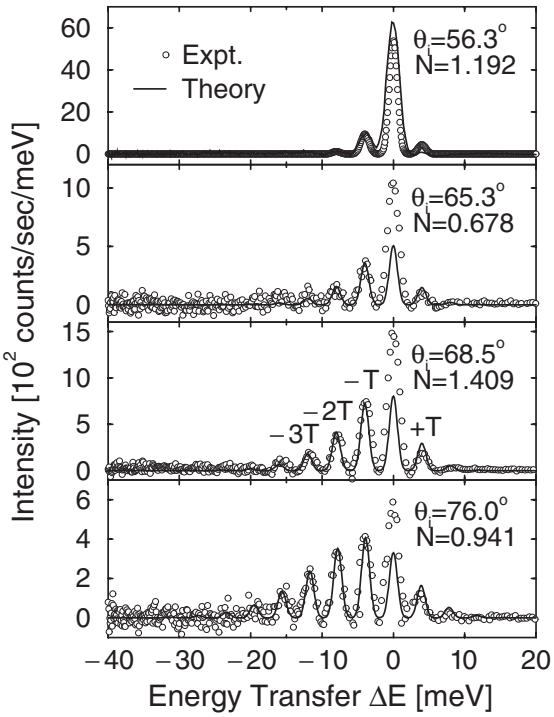

Figure 11. As figure 9, except with the incident energy at 66.6 meV, and incident angles from $\theta_i = 56.3^\circ$ to 76.0°.

However, for the two other incident angles which are much closer to specular, the values of $\Delta \boldsymbol{K}$ are much smaller and there is a large difference between the two calculations because the $|\Delta \boldsymbol{K}|^{-3}$ term in the form factor has a big effect and varies strongly from peak to peak. However, as shown in the right-hand panel of figure 14, when the form factor of equation (16) is included in the differential reflection coefficient, the results agree well with experiment. This agreement is important confirmation of the fact that Fraunhofer-like scattering from the hard repulsive molecular core is the most important term in the form factor describing inelastic scattering from adsorbed CO.

The applicability of the present theoretical approach was further tested by comparing the calculations obtained with equations (8) and (16) for CO/Cu(001) with CO/Pt(111). This provides a useful comparison, as shown in figure 5 for two TOF spectra measured for similar scattering conditions. As for CO/Cu(001), the present theoretical model accurately describes the intensity ratio of the observed inelastic peaks which, for these particular scattering conditions, are the fundamental and first-overtone energy loss peaks and the fundamental energy gain (phonon annihilation) peak of the 6 meV T-mode. The good quality of the fit provides additional support for the present theoretical model.

5.2. Intensities of scattering from Kr monolayers

The first step in the analysis is to fit the background-subtracted data at each incident angle and beam energy to the parameter-free theory obtained from equation (8) by using a constant form factor, i.e., taking $|\tau_{fi}|^2 = 1$. In order to match this parameter-free calculation to the

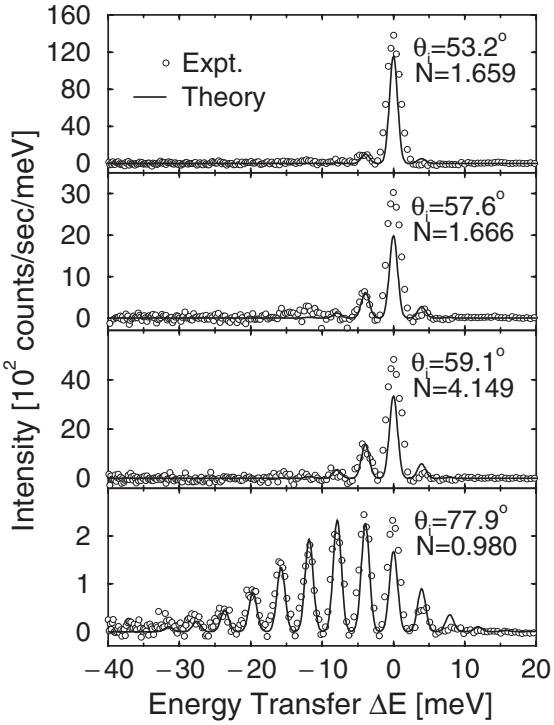

Figure 12. As figure 9, except with the incident energy at 83.4 meV, and incident angles from $\theta_i = 53.2^\circ$ to 77.9°.

data, at each energy and incident angle an overall normalization factor must be chosen to bring the calculations into the best fit with the data. These normalization factors, just as in the CO case above, when plotted as a function of incident angle or momentum transfer, become an effective 'form factor' that can be compared directly to the form factor chosen in equation (19). This is done in figure 15 where the normalization coefficients obtained by matching the $n = -1$ experimental peak intensities to the parameter-free theory are compared with $|\tau_{fi}|^2$ of equation (19) as a function of incident angle for the two measured incident energies. The normalization factors are shown as open circles connected by solid lines and the theoretical form factor is shown as a dashed curve, with the two parameters chosen as $\beta = 7.5$ Å^{-1} and $Q_0 = 5.5$ Å^{-1}. The agreement shown in figure 15 is reasonable, except when the incident angle is near the specular position at 47.9°, and this agreement provides experimental justification for the use of equation (19) for the form factor. The values of β and Q_0 are rather large compared to the typical values of $\beta \approx 2$ Å^{-1} and $Q_0 \approx 1$ Å^{-1} obtained from single-phonon inelastic He-atom scattering experiments on clean metal surfaces [40]; however, values even larger than this have been obtained for adsorbate-covered surfaces or under conditions for which many phonon quanta are exchanged in the collision. Large values of β and Q_0 imply a very hard repulsive barrier which is not unexpected for a rare-gas adsorbate layer. The repulsive part of the interaction potential is due to Pauli exchange repulsion between the surface and incoming projectile, and the Kr-electron distribution is tightly bound as opposed to the weakly bound free-electron distribution of a clean metal surface. For comparison, [30] gives a table of values of these parameters obtained from analysis of a large number of experiments, and it is seen that in many cases Q_0 and β are found to be as large as those values determined here.

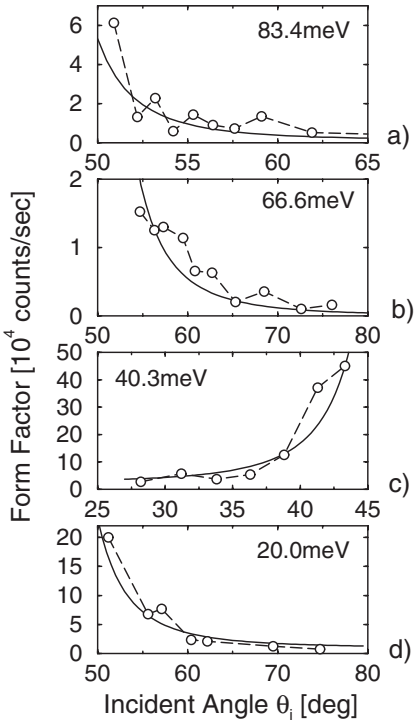

Figure 13. The experimentally obtained intensity of the $n = -1$ CO/Cu(001) T-mode phonon creation peak compared with the form factor of equation (16) for the incident energies (a) 83.4 meV, (b) 66.6 meV, (c) 40.3 meV, and (d) 20.0 meV. The experimental intensity is plotted as circles and the solid curve is the theoretical form factor for a hard-core radius of $a = 2.3$ Å.

The results of comparing the complete differential reflection coefficient of equation (8) with the form factor of equation (19) is presented in figures 16 and 17 as plots of intensity versus energy transfer for several selected incident angles at each of the two measured incident energies. The theoretical calculations are shown as solid curves in which the δ-function peaks of equation (8) have been broadened into Gaussians with a width given by the energy resolution of the incident beam. In the process of this final comparison with experiment it is necessary to multiply the calculated curves by an additional normalization factor close to unity in order to obtain the best fit. The need for this final renormalization is obvious from figure 15 because, although the calculated form factor follows the observed intensities reasonably well, the points are scattered about the theoretical curve. The value $\boldsymbol{N}$ chosen for this renormalization constant is shown in each panel of figures 16 and 17.

It is noticeable that, just as in the CO adsorbate case above, the peak for zero energy loss is where the biggest disagreement between theory and experimental intensities occurs. This is expected, because contributions to this peak come also from other sources, for example, the diffuse elastic scattering from defects and other impurities, e.g., a small fraction of coadsorbed CO, on the surface. For the surface considered here, the Kr monolayer is of very high quality; thus contributions from defects are expected to be smaller than for the case of isolated CO adsorbates. Under the assumption that the elastic scattering from defects is completely incoherent, this contribution would be expected to be purely additive and would make the $\Delta E = 0$ ($n = 0$) peak larger than predictions based on the elastic scattering from the S-mode.

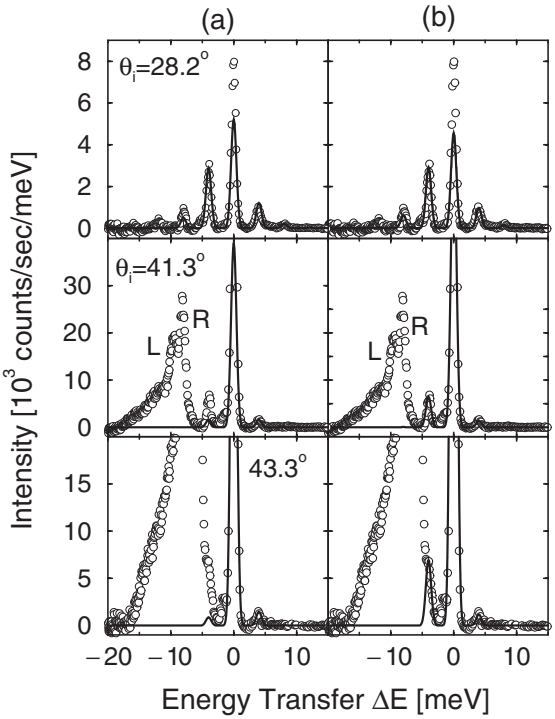

Figure 14. Comparison of the calculated inelastic multiphonon intensity (thick solid curve) with experimental data (circles) for $E_i = 40.29$ meV and selected incident angles. (a) shows the results of the calculations without including the scattering form factor of equation (16) while (b) shows the same calculations including this factor. At $\theta_i = 28.2^\circ$, which is far from specular conditions, the form factor is seen to have little effect. However, at $\theta_i = 41.3^\circ$ and 43.3°, which are close to specular and where the Fraunhofer term is dominant, the form factor has an important effect in bringing the calculated intensities for the inelastic overtone peaks into agreement with experiment. The two peaks marked L (longitudinal resonance) and R (Rayleigh mode) arise from the substrate vibrations.

This is indeed the case at the higher incident energy shown in figure 17; however, it is not always the situation at the lower incident energy as seen in figure 16 where especially at large incident angles the calculated elastic peak is considerably larger than the measured one. There can be several reasons for this discrepancy:

(1) In part this can be attributed to the normalization factor chosen for comparison of the calculations to the experimental data, although clearly this cannot explain all of the discrepancy.

(2) The elastic scattering from defects is certainly not completely incoherent, and the elastic scattering amplitudes can interfere destructively with themselves and even with the elastic scattering amplitude from the S-mode. Such destructive (and also constructive) interference effects are well known in He-atom scattering—such as the reflection symmetry oscillations observed in the diffuse elastic scattering from isolated adsorbates [27, 38].

(3) A third reason could be the neglect of the attractive adsorption well in the interaction potential. The well depth for He interacting with this surface is not known but can be estimated to be <10 meV. Nevertheless, this is a significant fraction of the incident energy

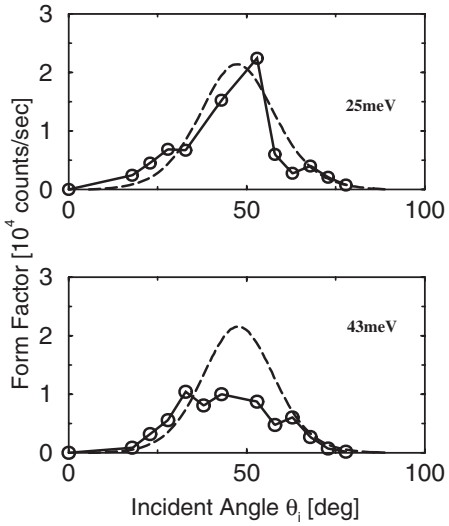

Figure 15. The experimentally obtained intensity of the $n = -1$ Kr/Pt(111) S-mode phonon creation peak compared with the form factor of equation (19) for the incident energies (a) 25 meV (upper panel) and (b) 43 meV (lower panel). The experimental intensities are plotted as circles connected by solid lines and the dashed curve is the theoretical form factor of equation (19) for an exponential repulsive wall.

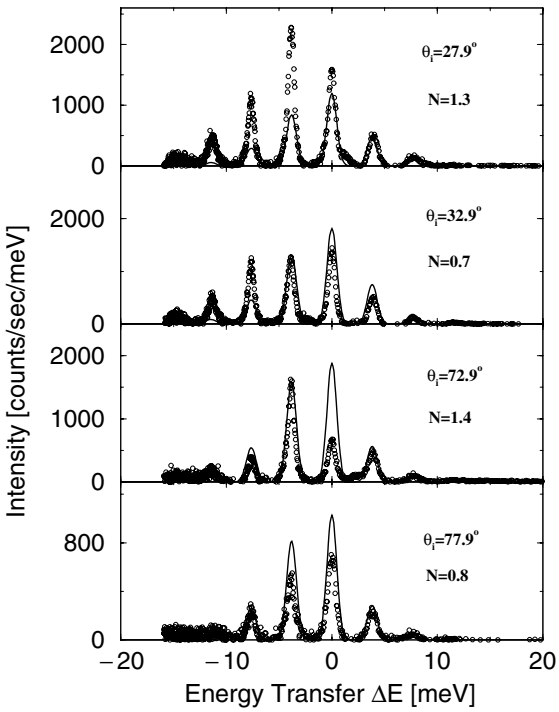

Figure 16. A series of inelastic HAS spectra for Kr on Pt(111) at $T_S = 58$ K and $E_i = 25.1$ meV as in figure 6, after background subtraction. The experimental points are shown as circles while the solid lines are the results of the theory.

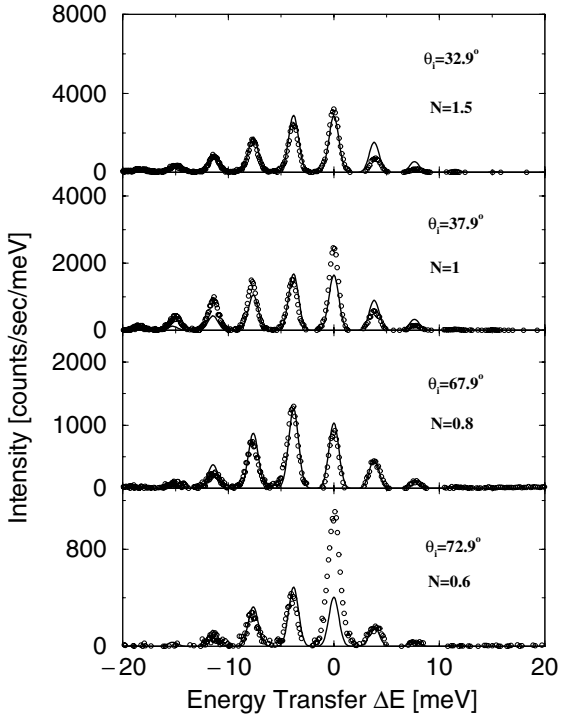

Figure 17. As figure 16, except with the incident energy at 43.0 meV.

of 25 meV and could be the cause of the less good agreement with the theory seen in figure 16 as compared to the higher incident energy of figure 17.

(4) A fourth possibility, also neglected here, is hybridization of the S-mode with the Rayleigh mode or bulk modes. Hybridization affects the phonons at small parallel wavevectors where the flat S-mode dispersion intersects with the dispersion curves of the Rayleigh and bulk modes. This can give rise, under conditions of multiple-phonon exchange, to broadening and subsequent reduced peak heights that affect the peak for zero energy loss differently from the higher-quantum-number peaks.

The overall agreement between theory and experiment exhibited in figures 16 and 17 is rather good. The theoretical model can be considered to have only two free parameters, aside from the renormalization constants which are nearly unity, and these two parameters are the Q_0 and β of the form factor. Thus, the essential features of the physical process leading to multiple overtones of the adsorbate S-mode appear to be contained in the generalized temperature-dependent Poisson distribution of equation (8) and the scattering form factor of equation (19). It is important to note that this theory provides a complete description at all incident angles with only a single normalization to bring theory into agreement with experiment, i.e., the different angular spectra are quantitatively predicted as shown in figure 15.

6. Predictions for the R- and S-modes of CO adsorbates

In the present experimental measurements on isolated adsorbates, and in previous investigations [10, 11, 15, 16, 38], no evidence for excitation of the R- or S-modes has been reported using He-atom scattering from CO adsorbates on either Cu or Pt surfaces. It is of

interest to examine the question of why this is the case with the present theoretical model in order to see whether one can predict experimental conditions under which these two modes might be observed.

Including the R- and S-modes in the theoretical model of equation (8) is relatively straightforward. Since these modes have frequencies considerably larger than that of the T-mode, it is expected that their intensities will be small and only the first-order energy loss contribution needs to be included, which is equivalent to calculating these intensities in a first-order Born approximation. However, higher-order overtones, and even cross-term contributions involving the simultaneous exchange of combinations of R-, S-, and T-mode quanta, are readily calculated within this formalism. The differential reflection coefficient for the scattering, including only the first-order contributions for the R- and S-modes, is

$$\begin{aligned}\frac{\mathrm{d}^3R(\boldsymbol{k}_f,\boldsymbol{k}_i)}{\mathrm{d}E_f\,\mathrm{d}\Omega_f} &= \frac{m^2}{(2\pi\hbar)^4}\frac{|\boldsymbol{k}_f|}{k_{iz}}|\tau_{fi}|^2\mathrm{e}^{-2W_T(\Delta\boldsymbol{K})}\mathrm{e}^{-2W_R(\Delta\boldsymbol{K})}\mathrm{e}^{-2W_S(k_z)}\mathrm{e}^{-2W(\boldsymbol{k})}\\ &\times\left\{\sum_{\alpha=-\infty}^{+\infty} I_{|\alpha|}\left(\frac{\Delta\boldsymbol{K}^2\hbar}{M_A\omega}\sqrt{n(\omega)[n(\omega)-1]}\right)\left(\frac{n(\omega)}{n(\omega)-1}\right)^{\alpha/2}\delta(E_f-E_i-\alpha\hbar\omega)\right.\\ &+ I_1\left(\frac{\Delta\boldsymbol{K}^2\hbar}{M_R\omega_R}\sqrt{n(\omega_R)[n(\omega_R)-1]}\right)\left(\frac{n(\omega_R)}{n(\omega_R)-1}\right)^{-1/2}\delta(E_f-E_i+\hbar\omega_R)\\ &\left.+ I_1\left(\frac{{k_z}^2\hbar}{M_S\omega_S}\sqrt{n(\omega_S)[n(\omega_S)-1]}\right)\left(\frac{n(\omega_S)}{n(\omega_S)-1}\right)^{-1/2}\delta(E_f-E_i+\hbar\omega_S)\right\}\end{aligned}\tag{21}$$

where $\exp\{-2W_R(\Delta\boldsymbol{K})\}$ is the contribution to the Debye–Waller factor arising from the R-mode, $\exp\{-2W_S(k_z)\}$ is the contribution to the Debye–Waller factor arising from the S-mode, and $\exp\{-2W_T(\Delta\boldsymbol{K})\}$ and $\exp\{-2W(\boldsymbol{k})\}$ are, as before, the contributions to the Debye–Waller factor arising from the T-mode and substrate modes, respectively.

Using the parameters for the existing experimental results, namely a total scattering angle of $\theta_{SD} = 95.8^\circ$ and incident energies up to 100 meV, equation (21) together with the form factor of equation (16) does not predict significant inelastic peak intensities for either the R- or S-modes, in agreement with the experimental observations. In fact, from the form of equation (21) it is clear why the high-energy modes have such small scattering intensities. First, the larger frequencies for ω_R and ω_S make the argument of the Bessel function and the value of the Bose–Einstein factor considerably smaller, making the intensity much smaller than for the T-mode despite the coupling of the S-mode to the larger perpendicular component of the momentum transfer k_z. Second, for the R-mode, as discussed in section 4.3 above, the normal-mode analysis gives a vibrational amplitude for the oxygen-atom vibration of $e(x,\mathrm{O},\mathrm{R})/e(x,\mathrm{C},\mathrm{R}) = -0.72$, as opposed to a value of $e(x,\mathrm{O},\mathrm{T})/e(x,\mathrm{C},\mathrm{T}) = +1.7$ for the T-mode. For the R-mode this translates into a large effective mass for the oxygen atom $M_R = M_\mathrm{O}/|e(x,\mathrm{O},\mathrm{R})|^2 = 16\ \mathrm{amu}/0.584^2 = 46.96$ amu, significantly reducing the calculated intensity and the contribution of the Debye–Waller factor. Similarly, as expected, it is found that the effective mass for the S-mode is close to the mass of the whole CO molecule, about twice the mass of an oxygen atom, $M_S = M_\mathrm{O}/|e(z,\mathrm{O},\mathrm{S})|^2 = 16\ \mathrm{amu}/0.721^2 = 30.78$ amu, which also tends to make the intensity of this mode smaller.

In particular for the R-mode, as noted earlier, the associated momentum transfer is the parallel component, while for the S-mode it is the perpendicular component. This has two important effects. First, the conditions in which the R-mode would produce large intensities, i.e., large parallel momentum transfers, will also be very favourable for the exchange of T-mode phonons. Thus, the lower frequency and smaller effective mass for the T-mode make it dominant. Further, the Debye–Waller contribution due to the T-mode will make both the

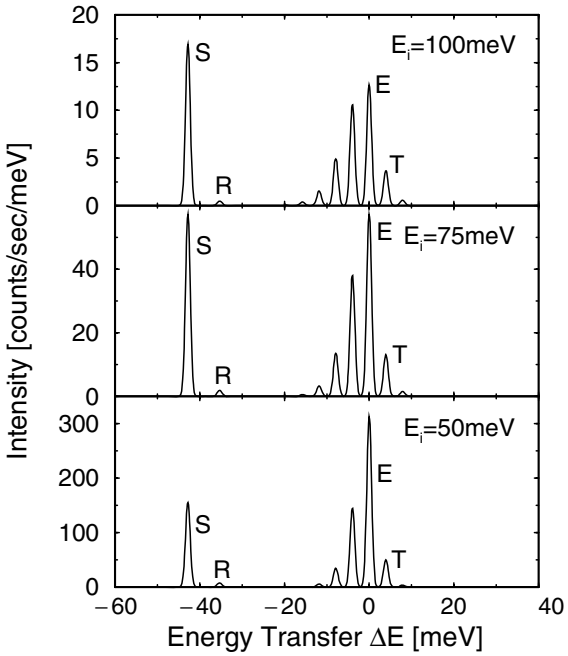

Figure 18. A series of calculated HAS inelastic spectra using realistic incident beam fluxes for isolated CO on Cu(001) at $T_S = 50$ K. The incident angle is $\theta_i = 22.5^\circ$ and the scattering angle is $\theta_f = 2.5^\circ$ corresponding to $\theta_{SD} = 25^\circ$. The incident energies range from 50 to 100 meV. In addition to the T-mode multiphonons at $\Delta E \approx \pm n \times 4$ meV, at $\Delta E \approx -35$ meV the contribution of the R-mode appears, and at $\Delta E \approx -43$ meV the contribution of the S-mode is observed as well.

R- and S-mode contributions small. This effect will make it particularly difficult to observe the R-mode, and probably explains why it has not yet been reported in He-atom experiments.

The perpendicular momentum transfer k_z associated with the S-mode should, on the other hand, help to make its intensity large. In the experiments shown in figures 9–12 the parallel momentum transfers are small and range up to 3–4 Å^{-1}, while the perpendicular components are typically larger than 10 Å^{-1}. Since these momentum transfers enter as squared terms in equation (21) this difference is substantially magnified. Thus, it would, at first, appear that the S-mode scattering intensity should be most observable under conditions in which the perpendicular momentum transfer is maximized and simultaneously the parallel momentum is minimized with the result that the T-mode contribution to the Debye–Waller attenuation is small. For the present experiments, this would correspond to incident angles near specular and a small angle θ_{SD} between the incident beam and detector, rather than the present angle of 95.8°.

A number of calculations were made using equation (21) for realistic experimental geometries which were anticipated to show the S-mode for CO/Cu(001). Figure 18 shows the predicted TOF spectra for incident helium-atom energies ranging from 50 to 100 meV and a small incident angle of $\theta_i = 22.5^\circ$ and with the detector placed at $\theta_f = 2.5^\circ$, making $\theta_{SD} = 25^\circ$. The calculations are scaled to represent a realistic incident beam flux by interpolating between the normalization factors for the experimental data given in figures 9–12. Thus, the calculated intensities shown in figure 18 are expected to represent realistic values realized for the present experimental apparatus with a smaller total scattering angle.

Under these conditions the S-mode peak at $\Delta E = -43$ meV exhibits a total integrated intensity relative to that of the sum of all in-plane T-mode overtones ranging from ≈25% at $E_i = 50$ meV to ≈50% at $E_i = 100$ meV. On the other hand, the R-mode peak, while clearly visible in the calculations, is no larger than the smallest of the non-negligible T-mode peaks. As the incident energy increases from 50 to 100 meV the relative intensities of both the T-mode and the S-mode peaks increase, but for the R-mode this increase is much less apparent. Note that the widths of the S- and R-mode peaks in figure 18 were chosen to be the same as that of the T-mode overtones, which is approximately the energy resolution of the experiment.

Consequently, we can conclude from the calculations that the S-mode of CO adsorbed on Cu(001) should be observable under conditions in which the parallel momentum transfer is small and the perpendicular momentum transfer is large, i.e., high incident energies and small incident and final scattering angles. However, if the parallel momentum transfer is non-negligible, even if it is significantly smaller than the perpendicular momentum transfer, the Debye–Waller factor due to the T-mode will be so small as to severely damp out the S-mode intensity. The R-mode, on the other hand, is predicted to be difficult to observe under almost all experimental conditions because large parallel momentum transfers are needed. Thus, as a result of the high frequency and higher effective mass of the R-mode and the significant T-mode multiphonon creation for large ΔK, the Debye–Waller factors for the R-mode are small, resulting in lower intensities.

7. Conclusions

Detailed experimental results have been reviewed for the multiple excitation of the parallel vibrational T-modes of CO adsorbed on Cu(001) and Pt(111), and for the vertically polarized S-modes of a monolayer of Kr on Pt(111). In each case the angular distribution of intensity into the multiphonon peaks was described in a simple way by a comprehensive scattering theory using only the most basic aspects of the interaction between helium atoms and the adsorbates. From a detailed comparison between the experimental results and theoretical calculations the following conclusions can be drawn:

(1) For both adsorbate systems the multiple-quantum intensity distribution is described well using a theory which is based on a generalized temperature-dependent Poisson distribution multiplied by a form factor which describes the interaction between the probe particle and the surface. In the case of isolated CO adsorbates, the form factor is that of a hard-core hemisphere on the surface representing the oxygen atom that the incoming He projectile strikes. All parameters associated with this hard-core potential have been determined in other experiments; thus the potential model for scattering from CO is one with no freely adjustable parameters. For the case of He scattering from the Kr monolayer, the form factor is chosen to be that of an exponentially repulsive barrier having two parameters, the exponential decay wavevector β and the cut-off parameter Q_0. As an additional point, all results depend only very slightly on the substrate Debye temperature because the substrate Debye–Waller factor has very little effect.

(2) The multiple-quantum excitations observed with HAS in all of these systems are equally spaced in energy, and exhibit no observable increase in peak width with overtone number. In the case of isolated CO adsorbates, the $n = -8$ T-mode peak, or seventh overtone, was observed at an energy loss of $\Delta E = -32$ meV. Since other experiments have shown that the CO/Cu(001) lateral potential is quite anharmonic and the diffusion barrier is only about 30 meV [15], the observed multiphonon excitations do not appear to be those of single molecules. This can be understood by considering that, just as in the case of helium

diffraction, single helium atoms interact with an area of the surface corresponding to the coherence width of the helium wavepackets, which is equivalent to the coherence width of the helium beam. Using a typical coherence width of 300 Å and the experimental CO coverage of $\Theta_{CO} = 0.03$ it can be seen that each helium atom interacts with about 330 CO molecules. Thus, even though the CO molecules are isolated, in the sense that there is no significant multiple scattering among them, this work provides strong evidence that the multiple-overtone energy transfer clearly must be a collective quantum effect. In the case of He scattering from the Kr monolayers, there is a measured value of 91.5 meV for the adsorption potential well depth of Kr/Pt(111) [44], and a theoretical prediction of 53.3 meV [45, 46]. Energy losses as great as $n = -5$, or 20 meV are observed at the higher incident energy of 43 meV in figure 17. This is a significant fraction of the adsorption potential and certainly is large compared to the diffusion barrier. Thus once again, the absence of observed anharmonicity supports the interpretation that the quantum excitations are, as expected, true phonon excitations involving large numbers of adsorbate atoms. These combined observations on two adsorbate systems with quite differently polarized Einstein-like modes indicate that these overtones are true 'phonon' modes, i.e., they are collective oscillations involving a very large number of adsorbates. Such a collective and coherent interpretation of the inelastic phonon loss spectra is consistent with a coherent quantum picture of the elastic diffraction of He atoms.

(3) It is of interest to note that the present theoretical formalism, through its dependence on momentum transfer, provides a clear method for determining the polarizations of Einstein-like dispersionless modes. There is a distinct signature difference between the results for S-mode excitation of the rare-gas monolayer, and those for the excitation of the frustrated translation parallel to the surface (T-mode) of isolated CO molecules. In the case of the Kr monolayer, figures 16 and 17 reveal that the number and relative intensities of the S-mode overtone peaks do not vary appreciably with incident beam angle. This follows directly from the fact that the exchange of perpendicular momentum in an experiment with a fixed angle between the incident beam and detector does not change appreciably with incident angle. For example, in this experiment where the fixed angle is approximately 90° the momentum transfer of the peak for zero energy loss can vary from approximately $\hbar k_i$, with the beam or detector at a grazing angle with respect to the surface plane, to approximately $\sqrt{2}\hbar k_i$ at specular conditions, a possible change of only about 40%. However, in the case of scattering from a T-mode such as that of adsorbed CO, the overtone intensities depend on the exchange of momentum parallel to the surface, and at the position of the peak for zero energy loss, this can vary from zero to approximately the momentum of the incident beam for a 90° fixed-angle experiment. For the T-mode results shown in figures 9–12 the number and relative intensity of the overtone peak intensities varied strongly with incident angle, with the smallest number of peaks observed near specular conditions where the parallel momentum transfer is small, and large numbers of peaks observed at large angular deviations away from specular where the parallel momentum transfer is large. Thus the signature distinction between the case of scattering from the perpendicular S-modes and parallel T-modes is very clear, and other mode polarizations should be recognizable simply from the behaviour of the peaks as a function of momentum transfer.

(4) The effective mass associated with each mode of vibration must be taken into account. For the cases of CO/Cu(001) and CO/Pt(111) this was achieved using a ball-and-spring model and fitting the force constants to the known isotope shift measurements. The good fit of the scattering theory to the experimental data showed, in addition, that the helium atoms probe the motion of the oxygen atom, which sits furthest out from the metal surface.

(5) The theory presented here has shown why, under the present experimental conditions, the S- and R-mode vibrations of adsorbed CO have not been observed to date even for experiments using incident energies considerably higher than the energy loss associated with these modes. It was found that, due to the near-90° geometry of current HAS experiments, the ratio of parallel to perpendicular momentum transfer favours the creation of T-mode multiphonons at the expense of the higher-frequency modes. It was shown that small incident and total scattering angles are more favourable for S-mode phonon creation which should be detectable under such conditions, whereas the R-mode is expected to be weak under almost all scattering conditions and probably undetectable.

Further information can be obtained about the response of the scattering intensity to mode polarization by observing the behaviour of the form factor. For isolated molecules, such as CO at low coverages considered here, the hard hemispherically shaped potential leads to a form factor which depends on the parallel momentum transfer according to $|\Delta K|^{-3}$ for intermediate values 0.3 Å$^{-1} \lesssim |\Delta K| \lesssim 2$ Å^{-1}. For low surface temperatures the Debye–Waller terms in equation (8) tend to unity and the creation of single T-mode phonons can be described by the I_1 modified Bessel function whose value is proportional to $|\Delta K|^2$. Thus, for intermediate parallel momentum transfers the fundamental T-mode intensity should follow a roughly $|\Delta K|^{-1}$ dependence. For a total scattering angle close to 90° the perpendicular momentum transfer k_z varies little with ΔK and the S-mode intensity is, consequently, dominated by the form factor term in equation 21, leading to a $|\Delta K|^{-3}$ dependence for intermediate $|\Delta K|$. Thus, the fundamental S-mode peak intensities for isolated CO adsorbates are expected to show a strong decrease in intensity as $|\Delta K|$ is increased away from specular, whereas the T-mode dependence is anticipated to be much weaker.

Finally, we would like to point out that the theoretical model used to analyse the present experimental results is not limited to the scattering of helium from specific adsorbate systems. The ease of application of this approach means that it can be used to predict the scattering interactions of other types of projectile with different molecular or atomic adsorbates. Furthermore, the incident conditions are not limited to well-defined monoenergetic beams but can also be used for less precise situations such as Maxwell–Boltzmann distributions of incident energies which are typical for realistic systems.

Acknowledgments

We would like to thank J P Toennies for support, encouragement and stimulating discussions. One of the authors (JRM) would like to thank the Max Planck Institut für Strömungsforschung for hospitality during the course of this work. This work was supported by the National Science Foundation under grant number DMR-0089503 and by the Department of Energy under grant number DE-FG02-98ER45704.

References

[1] Poelsema B and Comsa G 1989 *Scattering of Thermal Energy Atoms from Disordered Surfaces (Springer Tracts in Modern Physics vol 115)* (Berlin: Springer) p 1
[2] Braun J, Fuhrmann D, Siber A, Gumhalter B and Wöll Ch 1098 *Phys. Rev. Lett.* **80** 125
[3] Braun J, Fuhrmann D, Bertino M, Graham A P, Toennies J P, Wöll Ch, Bilic A and Gumhalter B 1997 *J. Chem. Phys.* **106** 9922
[4] Siber A, Gumhalter B, Braun J, Graham A P, Bertino M, Toennies J P, Fuhrmann D and Wöll Ch 1999 *Phys. Rev.* B **59** 5898
[5] Bruch L W, Graham A P and Toennies J P 2000 *J. Chem. Phys.* **112** 3314

[6] Saxena S C and Joshi R K 1989 *Thermal Accommodation and Adsorption Coefficients of Gases (CINDAS Data Series on Material Properties)* ed C Y Ho (New York: Hemisphere)
[7] Legge H, Toennies J P and Manson J R 1999 *J. Chem. Phys.* **10** 8767
[8] Hofmann F, Manson J R and Toennies J P 1996 *Surf. Sci.* **349** L184
[9] Mason B F and Williams B R 1983 *Surf. Sci.* **130** 295
[10] Lahee A M, Toennies J P and Wöll Ch 1986 *Surf. Sci.* **177** 371
[11] Ellis J, Toennies J P and Witte G 1995 *J. Chem. Phys.* **102** 5059
[12] Li M, Manson J R and Graham A P 2001 *Phys. Rev.* B **63** 155410
[13] Hirschmugl C J, Williams G P, Hoffmann F M and Chabal Y J 1990 *Phys. Rev. Lett.* **65** 480
[14] Truong C M, Rodriguez J A and Goodman D W 1992 *Surf. Sci. Lett.* **271** L385
[15] Graham A P, Hofmann F, Toennies J P, Williams G P, Hirschmugl C J and Ellis J 1998 *J. Chem. Phys.* **108** 7825
[16] Graham A P, Hofmann F and Toennies J P 1996 *J. Chem. Phys.* **104** 5311
[17] Schweizer E, Persson B N J, Tüshaus M, Hoge D and Bradshaw A M 1989 *Surf. Sci.* **213** 49
[18] Steininger H, Lehwald S and Ibach H 1982 *Surf. Sci.* **123** 264
[19] Graham A P and Toennies J P 1998 *Europhys. Lett.* **42** 449
[20] Manson J R and Skofronick J G 1993 *Phys. Rev.* B **47** 12 890
[21] Muis A and Manson J R 1997 *J. Chem. Phys.* **107** 1655
[22] Toennies J P 1988 *Springer Series in Surface Sciences* vol 14 (Berlin: Springer) p 248
Toennies J P 1991 *Surface Phonons (Springer Series in Surface Sciences vol 21)* ed W Kress and F W de Wette (Berlin: Springer) p 111
Toennies J P 1993 *J. Phys.: Condens. Matter* **5** A25
[23] Hofmann F, Toennies J P and Manson J R 1994 *J. Chem. Phys.* **101** 10 155
[24] Poelsema B, de Zwart S T and Comsa G 1982 *Phys. Rev. Lett.* **49** 578
Poelsema B, de Zwart S T and Comsa G 1983 **51** 522
[25] Bertino M, Ellis J, Hofmann F, Toennies J P and Manson J R 1994 *Phys. Rev. Lett.* **73** 605
[26] Braun J, Graham A P, Hofmann F, Silvestri W, Toennies J P and Witte G 1996 *J. Chem. Phys.* **105** 3258
[27] Lahee A M, Manson J R, Toennies J P and Wöll Ch 1986 *Phys. Rev. Lett.* **57** 471
Lahee A M, Manson J R, Toennies J P and Wöll Ch 1987 *J. Chem. Phys.* **86** 7194
[28] Graham A P, Hofmann F, Toennies J P and Manson J R 1996 *J. Chem. Phys.* **105** 2093
[29] Kern K, Zeppenfeld P, David R and Comsa G 1987 *Phys. Rev.* B **35** 886
[30] Hofmann F, Toennies J P and Manson J R 1997 *J. Chem. Phys.* **106** 1234
[31] Rodberg L S and Thaler R M 1967 *Quantum Theory of Scattering* (New York: Academic)
[32] Manson J R 1991 *Phys. Rev.* B **43** 6924
[33] Bertino M F, Manson J R and Silvestri W 1998 *J. Chem. Phys.* **108** 10 239
[34] Brako R and Newns D M 1982 *Phys. Rev. Lett.* **48** 1859
Brako R and Newns D M 1982 *Surf. Sci.* **123** 439
[35] Manson J R 1994 *Comput. Phys. Commun.* **80** 145
[36] Manson J R 1988 *Phys. Rev.* B **37** 6750
[37] Lemoine D 1994 *J. Chem. Phys.* **101** 4343
[38] Choi B H, Tang K T and Toennies J P 1997 *J. Chem. Phys.* **107** 1631
Choi B H, Tang K T and Toennies J P 1997 *J. Chem. Phys.* **107** 9437
[39] Morse P M and Feshbach H 1953 *Methods of Theoretical Physics* (New York: McGraw-Hill) p 1554
[40] Celli V, Benedek G, Harten U and Toennies J P 1984 *Surf. Sci. Lett.* **143** L376
[41] Jackson J M and Mott N F 1932 *Proc. R. Soc.* A **137** 703
[42] Goodman F O and Wachman H Y 1976 *Dynamics of Gas–Surface Scattering* (New York: Academic)
[43] Celli V, Himes D, Tran P, Toennies J P, Wöll Ch and Zhang G 1991 *Phys. Rev. Lett.* **66** 3160
[44] Chon H, Fisher R A, McGammon R D and Aston J G 1962 *J. Chem. Phys.* **36** 1378
[45] Kleiman G G and Landman U 1976 *Solid State Commun.* **18** 819
[46] Vidali G, Ihm G, Kim H-Y and Cole M W 1991 *Surf. Sci. Rep.* **12** 133